Am J Physiol Lung Cell Mol Physiol 325: L508–L517, 2023.
First published August 29, 2023; doi:10.1152/ajplung.00101.2023

american physiological society

AMERICAN JOURNAL OF PHYSIOLOGY
LUNG CELLULAR AND MOLECULAR PHYSIOLOGY

RESEARCH ARTICLE

Novel Insights into Preterm Respiratory Physiology: Celebrating the 100th Birthday of Dr. Mildred T. Stahlman

Constrained drop surfactometry for studying adsorbed pulmonary surfactant at physiologically relevant high concentrations

Xiaojie Xu,[1] Guangle Li,[1] and Yi Y. Zuo[1,2]

[1]*Department of Mechanical Engineering, University of Hawaii at Manoa, Honolulu, Hawaii, United States and* [2]*Department of Pediatrics, John A. Burns School of Medicine, University of Hawaii, Honolulu, Hawaii, United States*

Abstract

Exogenous surfactant therapy has been used as a standard clinical intervention for treating premature newborns with respiratory distress syndrome. The phospholipid concentrations of exogenous surfactants used in clinical practice are consistently higher than 25 mg/mL; while it was estimated that the phospholipid concentration of endogenous surfactant is approximately in the range between 15 and 50 mg/mL. However, most in vitro biophysical simulations of pulmonary surfactants were only capable of studying surfactant concentrations up to 3 mg/mL, one order of magnitude lower than the physiologically relevant concentration. Using a new in vitro biophysical model, called constrained drop surfactometry, in conjunction with atomic force microscopy and other technological advances, we have investigated the biophysical properties, ultrastructure, and topography of the pulmonary surfactant film adsorbed from the subphase at physiologically relevant high surfactant concentrations of 10–35 mg/mL. It was found that the effect of surfactant concentration on the dynamic surface activity of the surfactant film was only important when the surface area of the surfactant film varied no more than 15%, mimicking normal tidal breathing. The adsorbed surfactant film depicts a multilayer conformation consisting of a layer-by-layer assembly of stacked bilayers with the height of the multilayers proportional to the surfactant concentration. Our experimental data suggest that the biophysical function of these multilayer structures formed after de novo adsorption is to act as a buffer zone to store surface-active materials ejected from the interfacial monolayer under extreme conditions such as deep breathing.

NEW & NOTEWORTHY An in vitro biophysical model, called constrained drop surfactometry, was developed to study the biophysical properties, ultrastructure, and topography of the pulmonary surfactant film adsorbed from the subphase at physiologically relevant high surfactant concentrations of 10–35 mg/mL. These results suggest that the biophysical function of multilayers formed after de novo adsorption is to act as a buffer zone to store surface-active materials ejected from the interfacial monolayer under extreme conditions such as deep breathing.

atomic force microscopy; constrained drop surfactometry; pulmonary surfactant; surface tension; ultrastructure

INTRODUCTION

Pulmonary surfactant is a lipid–protein complex synthesized by the alveolar type II epithelial cells (1). It forms a thin film at the air–water surface of the lungs via rapid adsorption, immediately after inflating the lungs with air on the newborn's first breath (2). The adsorbed pulmonary surfactant film plays a dual physiological role of host defense against inhaled particles and pathogens, and surface tension reduction that increases lung compliance and stability of the alveolar architecture (3). Deficiency or dysfunction of endogenous pulmonary surfactant leads to life-threading respiratory diseases (4). Neonatal respiratory distress syndrome (RDS) is a major disease of surfactant deficiency caused by premature birth (5). In addition to assisted ventilation and continuous positive airway pressure, surfactant replacement has been used as a standard clinical intervention to treat premature newborns with or at high risk for RDS (6). Surfactant replacement therapy has also been attempted to treat pediatric and adult patients with acute respiratory distress syndrome (ARDS) (7), but with only limited success (8). Amid the COVID-19 pandemic, surfactant replacement has been tested as a supportive therapy to treat patients with COVID-19-induced ARDS (9, 10).

Several in vitro biophysical models have been developed to assess the dynamic surface activity of pulmonary surfactant preparations. The three most widely used in vitro methods are the Langmuir film balance, pulsating bubble

Correspondence: Y. Y. Zuo (yzuo@hawaii.edu).
Submitted 30 March 2023 / Revised 15 July 2023 / Accepted 24 August 2023

surfactometry (PBS), and captive bubble surfactometry (CBS). Compared with the other two methods, the Langmuir film balance is usually only used for studying the compression of surfactant monolayers spread with an organic solvent, and thus has only limited capacity for biophysical simulations (1). The PBS determines the minimum and maximum surface tensions of pulmonary surfactant by oscillating a small air bubble (~1 mm in diameter) suspended in pulmonary surfactant, with a fixed rate of 20 cycles/min and a fixed surface area reduction of 50% (11). Because of its simplicity and small sample consumption (~20 μL), PBS has gained popularity in medical research and quality control of clinical surfactant preparations (12). Nevertheless, the PBS only provides approximate biophysical simulations of pulmonary surfactant, mostly because of film leakage at the capillary tube to which the air bubble is suspended (1). To reduce surface tension to physiologically relevant low values, the surfactant film in PBS needs to be compressed and expanded up to 100 cycles, i.e., 5 min, and in each cycle, the surfactant film is compressed by 50% of its initial surface area, which has little physiological relevance since the surface area of the lungs does not vary more than 20% during normal tidal breathing (13).

The CBS is the first in vitro model capable of simulating the biophysical properties of pulmonary surfactant films under physiologically relevant conditions (14). It uses a large air bubble of 2–7 mm in diameter floating in a few milliliters of the surfactant suspension held in a transparent chamber. The bubble is separated from the chamber's ceiling, treated with a hydrophilic coating, by a thin wetting film, and hence, the bubble is "captured" by the liquid phase, thus eliminating all potential pathways for film leakage (15). The CBS is capable of assaying the biophysical properties of adsorbed pulmonary surfactant films undergoing dynamic compression-expansion cycles that simulate tidal breathing (16, 17). In spite of its superb performance in biophysical simulations, the CBS has a technical limitation in studying pulmonary surfactants. The surfactant suspension becomes murky or even opaque at high concentrations, which makes surface tension measurements from the shape of the bubble challenging or even impossible (18, 19). Consequently, the maximum surfactant concentration that can be in vitro simulated with the CBS is usually no more than 3 mg/mL (16, 17). This technical limitation can be somehow circumvented by spreading a high-concentration aqueous surfactant suspension around the bubble surface using a micro syringe, and meanwhile, modifying the saline subphase with 10 wt% sucrose to help reduce precipitation of the surfactant vesicles (20).

The surfactant concentration used in clinical preparations varies but is consistently higher than 25 mg of phospholipids per milliliter (6). Survanta, a bovine surfactant prepared from minced lung tissues and supplemented with synthetic dipalmitoyl phosphatidylcholine (DPPC), palmitic acid, and tripalmitin, is clinically used at a concentration of 25 mg/mL. BLES, a bovine surfactant extracted from the lunge lavage of adult cows, is clinically used at 27 mg/mL. Infasurf, a bovine surfactant prepared from the lung lavage of newborn calves, is used at 35 mg/mL. Curosurf, a porcine surfactant prepared from minced lung tissues, is used at a high lipid concentration of 80 mg/mL.

The concentration of endogenous pulmonary surfactant in the alveolar hypophase of adult mammals could be estimated based on the total surfactant phospholipids recovered from bronchoalveolar lavage (21–23), the alveolar surface areas of various mammal species (24), and the overall area-weighted average thickness of the alveolar lining layer (i.e., 0.2 μm) (25). Based on these data, it can be estimated that the endogenous surfactant concentration in adult mammals' lungs likely ranges between ~15 and ~50 mg/mL. To the best of our knowledge, in vitro biophysical simulations of pulmonary surfactants at these physiologically relevant high concentrations (i.e., >10 mg/mL) are still scarce.

Here, we report in vitro biophysical simulations of an animal-derived natural pulmonary surfactant, Infasurf, at the physiologically relevant high surfactant concentrations up to 35 mg/mL, using a novel experimental methodology called constrained drop surfactometry (CDS), developed in our laboratory (26). The CDS is capable of simulating the intra-alveolar microenvironment of pulmonary surfactants under physiologically relevant conditions. We have recently developed a novel subphase replacement technique and an in situ Langmuir–Blodgett (LB) transfer technique that allows direct atomic force microscopy (AFM) imaging of the ultrastructure and topography of adsorbed pulmonary surfactant films with submicron resolutions (27). These findings have novel implications for a better understanding of the physiological and biophysical functions of the pulmonary surfactant film and may offer new translational insights into the design of clinical surfactant preparations to treat respiratory distress syndrome.

MATERIALS AND METHODS

Pulmonary Surfactant

Infasurf was a gift from ONY Biotech (Amherst, NY). It is prepared from the lung lavage of newborn calves with centrifugation and organic extraction. Infasurf contains all hydrophobic components of the natural bovine surfactant, whereas hydrophilic surfactant proteins (SP-A and SP-D) were removed during the extraction process. Infasurf was stored at −20°C in sterilized vials with an initial phospholipid concentration of 35 mg/mL. It was diluted with a saline buffer to various phospholipid concentrations on the day of the experiment.

Constrained Drop Surfactometry

Constrained drop surfactometry (CDS) is a new generation of droplet-based tensiometry technique developed in our laboratory for biophysical simulations of pulmonary surfactants (26, 28). As illustrated in Fig. 1, the CDS uses the air–water surface of a sessile droplet (~3 mm in diameter, ~0.14 cm^2 in surface area, and ~7 μL in volume) to accommodate the adsorbed surfactant film. The size of the droplet is about one order of magnitude larger than the size of individual alveoli (~200 μm) but is within the same order of magnitude as the size of the bubble used in PBS (~ 1 mm) and CBS (2–7 mm). The surfactant droplet is constrained on a carefully machined pedestal that uses its knife-sharp edges to prevent film leakage, even at low surface tensions. The adsorbed surfactant film can be compressed and expanded periodically at physiologically relevant rates and compression ratios by controlling liquid flow out of and into the droplet using a

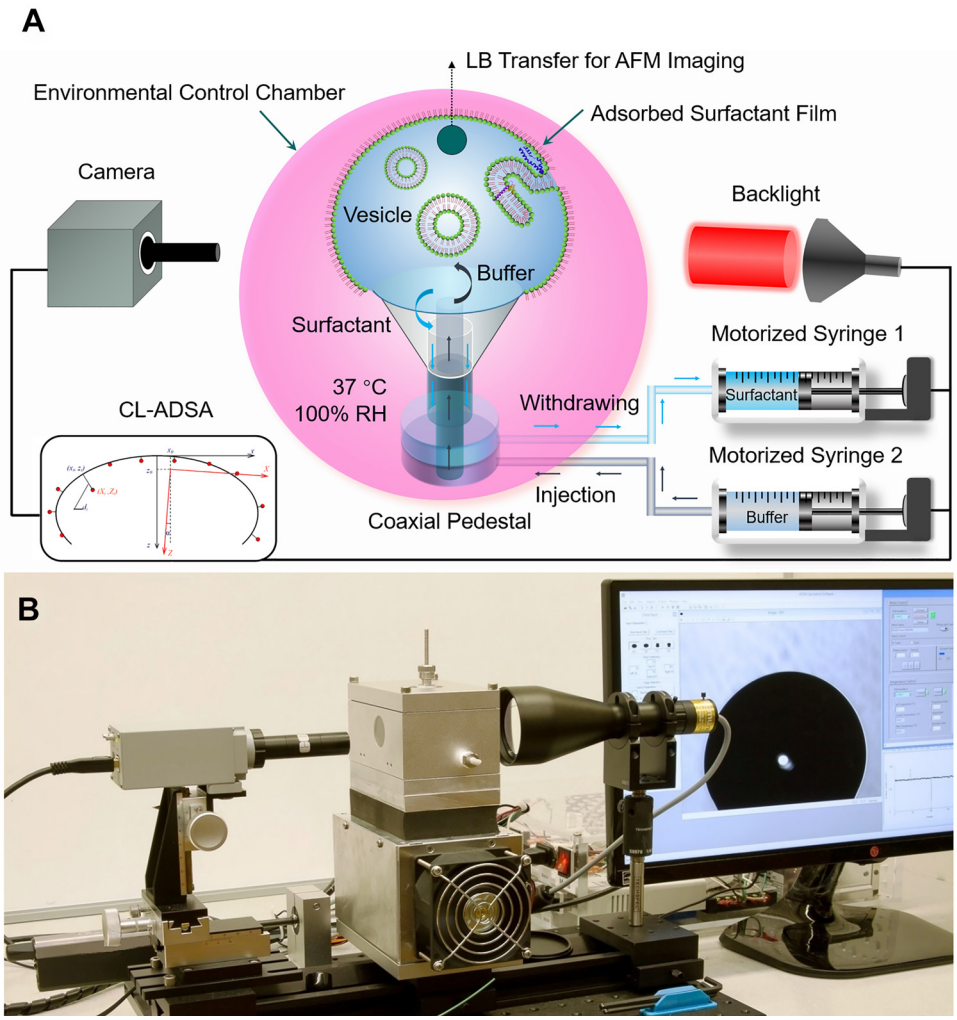

Figure 1. *A*: schematic of the constrained drop surfactometry (CDS). Pulmonary surfactant is adsorbed to the air-water interface of a surfactant droplet. The sessile droplet is constrained on a 3-mm pedestal with knife-sharp edges and is enclosed in an environmental control chamber maintained at 37°C and 100% relative humidity (RH). Surface tension and surface area of the adsorbed surfactant film are determined simultaneously from the shape of the droplet using closed-loop axisymmetric drop shape analysis (CL-ADSA). Subphase replacement is implemented with a coaxial pedestal connected to two motorized syringes, with one withdrawing the vesicle-containing subphase from the droplet and another one simultaneously injecting buffer into the droplet with the same volumetric rate. The adsorbed surfactant film is subsequently Langmuir–Blodgett (LB) transferred from the air-water interface to a freshly peeled mica substrate for atomic force microscopy (AFM) imaging. *B*: a picture of the constrained drop surfactometry (CDS) setup.

motorized syringe. The surface tension and surface area of the adsorbed surfactant film are determined from the shape of the droplet using closed-loop axisymmetric drop shape analysis (CL-ADSA) (29). Owing to system miniaturization, the CDS enables a high-fidelity simulation of the intra-alveolar environment, including the core body temperature of 37°C and a relative humidity close to 100%, using an environmental control chamber.

Specifically, a 7-μL Infasurf droplet, with a specific surfactant concentration, was dispensed onto the CDS pedestal using a micropipette. Immediately after dispensing the droplet, its surface tension was continuously recorded and was found to quickly (within seconds) reduce to an equilibrium value around 22–25 mN/m, indicating rapid adsorption of the pulmonary surfactant film at the air–water surface of the droplet (1). To mimic exhalation and inhalation, the adsorbed surfactant film was compressed and expanded at 20 cycles per minute with the compression ratios controlled at 15%, 25%, and 35%, respectively.

Subphase Replacement and Langmuir–Blodgett Transfer

To facilitate direct imaging of the ultrastructure and topography of the adsorbed surfactant film, we have developed a novel subphase replacement technique and an in situ Langmuir–Blodgett (LB) transfer technique (27). As shown in Fig. 1, the subphase replacement was implemented using a coaxial CDS pedestal connected with two motorized syringes, with one withdrawing the phospholipid-vesicle-containing subphase from the droplet at a flowrate of 10 μL/s, and the other one simultaneously injecting buffer into the droplet with the same flowrate. Consequently, phospholipid vesicles in the aqueous subphase, i.e., the droplet, were washed away without disturbing the adsorbed Infasurf film at the air–water surface. After the subphase replacement, LB transfer of the adsorbed Infasurf film was performed by first quickly inserting a freshly peeled mica sheet into the droplet, followed by slowly lifting the mica across the air–water surface of the droplet at a rate of 1 mm/min. During the LB transfer process, the Infasurf film was maintained at a constant surface pressure (±1 mN/m) using CL-ADSA. All measurements were conducted at 37°C at least three times. The deposition ratio of the LB transfer, defined as the ratio between the lost area of the surfactant film during the LB transfer and the total surface area of the mica sheet (30), was estimated to be ~1.24 (27), thus indicating a complete transfer of the surfactant film from the air–water surface to the mica surface.

Atomic Force Microscopy

The ultrastructure and topography of the adsorbed surfactant films were imaged using Innova atomic force microscopy (AFM; Bruker, Santa Barbara, CA). Samples were scanned in the air using the tapping mode with a silicon cantilever of the spring constant 42 N/m and a resonance frequency of 300 kHz. Images were taken at multiple locations to ensure reproducibility. Lateral structures, topography, bearing area, and bearing volume of the surfactant samples were analyzed using NanoScope Analysis (version 1.5).

Statistics

Samples from various batches were studied. All results are shown as means ± SD ($n > 3$). Nonparametric Kruskal–Wallis test was used to determine group differences (OriginPro, Northampton, MA). $P < 0.05$ was considered to be statistically significant.

RESULTS

Dynamic Surface Activity of the Adsorbed Surfactant Film

Figure 2 shows the dynamic surface activity of the Infasurf film adsorbed at physiologically relevant phospholipid concentrations of 10, 20, and 35 mg/mL. A relatively low surfactant concentration of 1 mg/mL was also studied as a reference. The reproducibility of these dynamic surface tension measurements can be found in Supplemental Fig. S1. Three area compression ratios, i.e., 15%, 25%, and 35%, were studied. The dynamic surface activity of the adsorbed

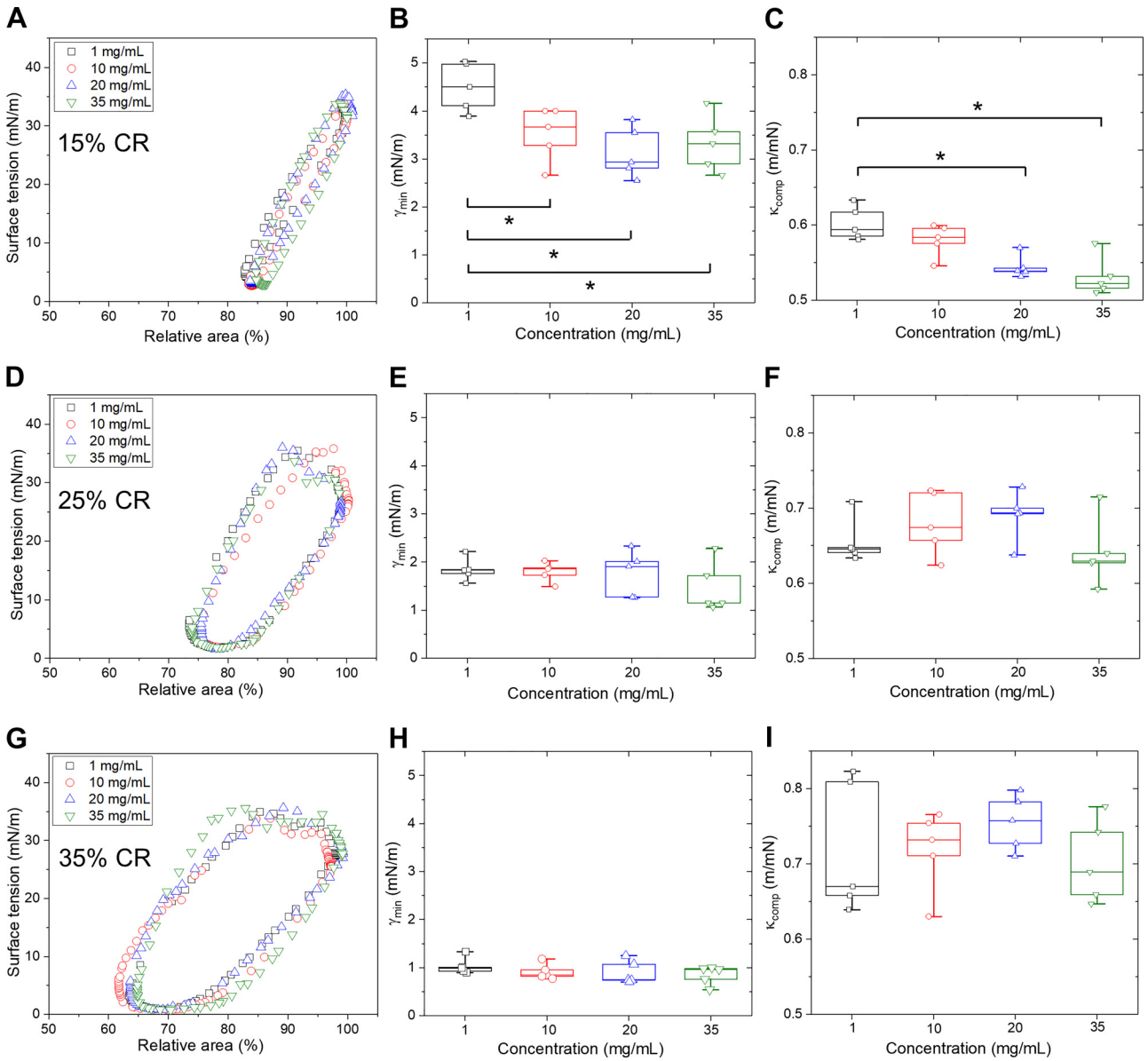

Figure 2. Dynamic surface activity of the Infasurf film adsorbed from a series of phospholipid concentrations, i.e., 1, 10, 20, and 35 mg/mL. Results shown are typical compression–expansion cycles (the 10th cycle), minimum surface tension (γ_{min}), and film compressibility (κ_{comp}) for 3 different film compression ratios (CRs), i.e., 15% (*A–C*), 25% (*D–F*), and 35% (*G–I*). All dynamic cycling experiments were performed at 37°C with a cycling rate of 3 s per cycle using the CDS. *$P < 0.05$ in comparison with Infasurf at the phospholipid concentration of 1 mg/mL.

surfactant film was quantified with the minimum surface tension (γ_{min}) and the film compressibility (κ_{comp}), all based on data of the 10th consecutive cycle.

As shown in Fig. 2, *A–C*, at the physiologically relevant 15% compression ratio, the γ_{min} of Infasurf at 1 mg/mL, is 4.5 mN/m. When the surfactant concentration is increased to 10, 20, and 35 mg/mL, the γ_{min} is reduced to 3.5, 3.1, and 3.0 mN/m, respectively, all below 4 mN/m. The κ_{comp} of the Infasurf film at 1 mg/mL is 0.60 m/mN, which gradually decreases to 0.52 m/mN, when the surfactant concentration is increased to 35 mg/mL. At the 25% compression ratio (Fig. 2, *D–F*), the γ_{min} of Infasurf at all studied concentrations is consistently lower than 2 mN/m. The κ_{comp} of the Infasurf film varies between 0.65 and 0.70 m/mN. No statistically significant differences can be found among various concentrations from 1 to 35 mg/mL. At the 35% compression ratio (Fig. 2, *G–I*), the γ_{min} of Infasurf at all studied concentrations reaches values lower than 1.0 mN/m, and the κ_{comp} varies between 0.7 and 0.8 m/mN, without statistically significant differences among these surfactant concentrations.

Optimization of the Subphase Replacement for AFM Imaging

For imaging the ultrastructure and topography of the adsorbed surfactant film, subphase replacement is needed to wash away the nonadsorbing phospholipid vesicles from the droplet. Otherwise, the solid substrate for LB transfer would be contaminated before the LB transfer, thus compromising the quality of AFM imaging. A key parameter that affects the subphase replacement process is the replacement volume. An optimal replacement volume should be the minimum volume capable of removing all nonadsorbing vesicles from the droplet, while effectively preserving the structure and functionality of the multilayer structures of the adsorbed surfactant film (27). For the Infasurf film adsorbed from a relatively low phospholipid concentration of 1 mg/mL, our previous study has determined the optimal subphase replacement volume to be threefold (3X) of the droplet volume (27).

Figure 3 shows the optimization process for the Infasurf film adsorbed from a phospholipid concentration of 10 mg/mL. The reproducibility of these AFM images can be found in Supplemental Figs. S2–S9. It can be seen that subphase replacement from 5× to 20× volumes did not effectively remove all vesicles. Large unilamellar and multilamellar vesicular structures with a height range between 200 and 300 nm were found to adsorb to the mica surface. With the 25× replacement volume, the AFM images demonstrate well-organized multilayer structures consisting of bilayer stacks of 60–90 nm in height (see Fig. 4*B* for detailed topographic analysis). With the 35× replacement volume, the adsorbed Infasurf film also shows an organized multilayer structure. However, with further increasing the replacement volumes to 40X and 45X, the adsorbed Infasurf film depicts a primary monolayer conformation with only isolated multilayer protrusions, thus indicating compromised multilayer structures due to excessive washing. These AFM observations, therefore, collectively indicate that the optimal subphase replacement volume for imaging 10 mg/mL Infasurf is around 25×, which balances the sufficient removal of nonadsorbing vesicles from the droplet and the effective preservation of functional multilayer structures.

A similar optimization process has been performed for imaging the Infasurf film adsorbed from 20 and 35 mg/mL surfactant suspensions, respectively. As shown in Supplemental Fig. S10, the optimal replacement volumes for 20 and 35 mg/mL Infasurf were found to be 45× and 80×, respectively. Taking together, a linear calibration curve has been produced to determine the optimal subphase replacement volume for imaging adsorbed surfactant films, as a function of the subphase phospholipid concentration (Supplemental Fig. S11).

Ultrastructure and Topography of the Adsorbed Surfactant Film

Figure 4 shows the ultrastructure and topography of the Infasurf film adsorbed from the surfactant concentrations of 1, 10, 20, and 35 mg/mL, respectively. As shown in Fig. 4*A*, at a low concentration of 1 mg/mL, the Infasurf film shows a large number of uniformly distributed protrusions between 16 and 28 nm in height. Given the thickness of a fully hydrated phospholipid bilayer to be around 4 nm (31), these protrusions correspond to 4–7 stacked bilayers, in good agreement with our previous observation of the adsorbed Infasurf film from the same surfactant concentration, i.e., 1 mg/mL (27).

Increasing the surfactant concentration to physiologically relevant levels, the adsorbed Infasurf film demonstrates significantly larger multilayer structures both in the lateral and height dimensions. These multilayer structures depict a well-defined conformation of layer-by-layer assembly of stacked bilayers with the height of the multilayers proportional to the surfactant concentration of the subphase. The height profile of these multilayers shows a stair-like structure with the height of each "stair" to be a multiplier of ~4 nm (i.e., the thickness of a single bilayer).

Figure 5 shows the statistical analysis of the maximum height, the area fraction, and the surface area-averaged equivalent number of phospholipid bilayers stored in the multilayers of the Infasurf film adsorbed from various surfactant concentrations. Supplemental Fig. S12 shows an example how bearing analysis of the AFM images was performed. The maximum height of the multilayer structure is 36, 96, 148, and 228 nm, corresponding to stacks of 9, 24, 37, and 57 lipid bilayers, for the Infasurf film adsorbed from the surfactant concentrations of 1, 10, 20, and 35 mg/mL, respectively. The area fraction of the multilayers increases from 9% of the entire surfactant film at 1 mg/mL, to ~70% at 35 mg/mL. The equivalent number of phospholipid bilayers stored in the multilayers of the Infasurf film, averaged over the entire surface area of the adsorbed Infasurf film, can be estimated from the volume of all multilayer structures found in the Infasurf film with a surface area of $20 \times 20\ \mu m^2$. The equivalent number of phospholipid bilayers stored in the multilayers is found to be 0.7, 3.1, 3.9, and 4.6 bilayers for surfactant concentrations of 1, 10, 20, and 35 mg/mL, respectively.

DISCUSSION

High Phospholipid Concentration Optimizes Surface Activity of the Surfactant Film during Normal Tidal Breathing

Using CDS, we have studied the dynamic surface activity of the Infasurf film adsorbed from surfactant suspensions at

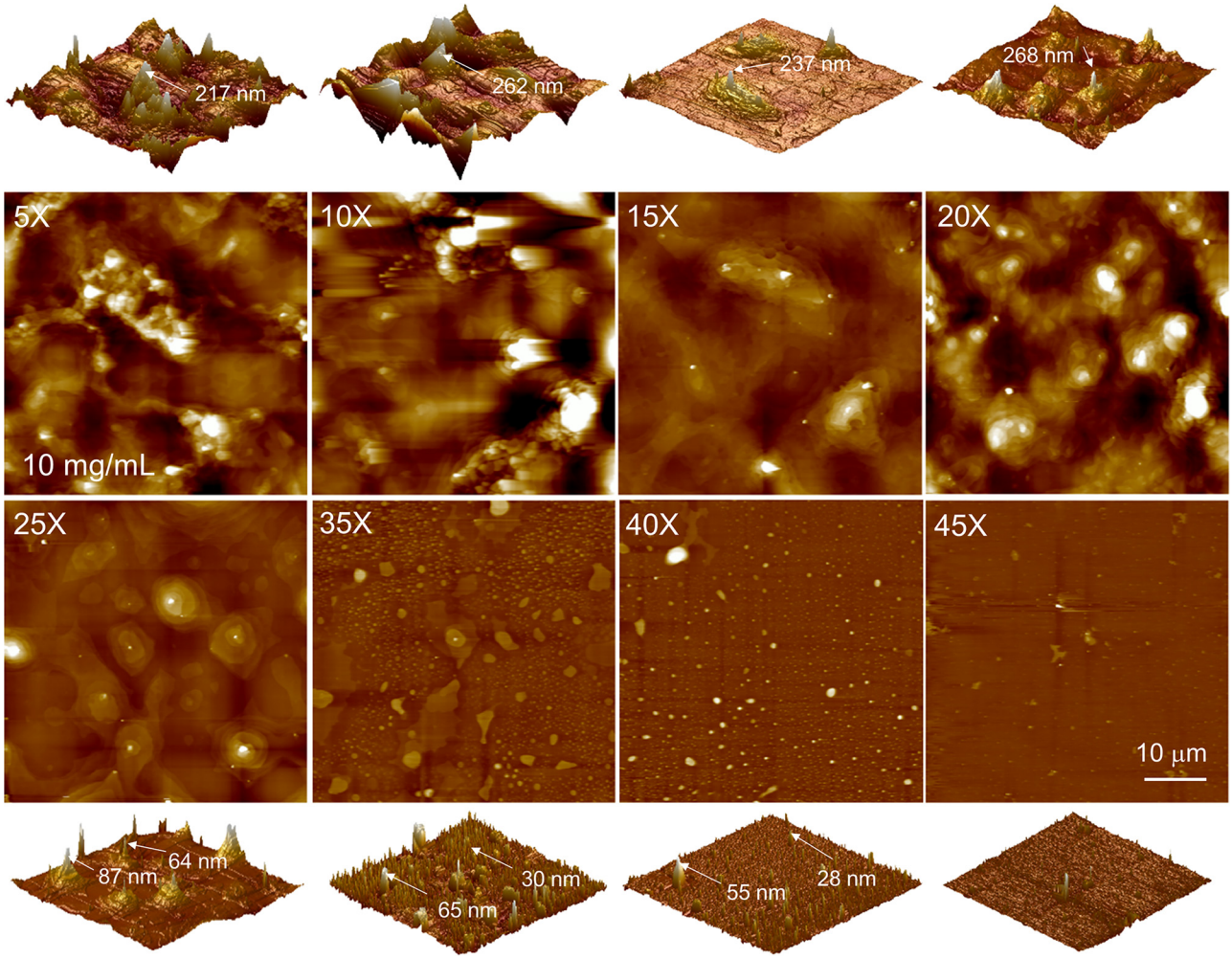

Figure 3. Ultrastructure and topography of the Infasurf film after de novo adsorption from a phospholipid concentration of 10 mg/mL. Atomic force microscopy (AFM) images of the adsorbed surfactant film were obtained after subphase replacement with buffer volumes from fivefold (5X) to 45-fold (45×) of the original droplet volume. Images in the *top* and *bottom* rows show the three-dimensional (3-D) rendering of the corresponding two-dimensional (2-D) AFM images shown in the *middle* rows. All AFM images have the same scanning area of 50 × 50 μm. AFM images for 5×, 10×, 15×, and 20× have a *z* range of 200 nm. AFM images for 25× and 35× have a *z* range of 100 nm, whereas the *z* range for the images of 40× and 45× is 30 nm. The 25× replacement volume was found to be an optimal subphase replacement volume because it efficiently removed the nonadsorbing vesicles from the droplet and, meanwhile, preserved the multilayers of the adsorbed Infasurf film. Arrows indicate the heights of structures.

the physiologically relevant phospholipid concentrations, i.e., ≥10 mg/mL (Fig. 2). Two conclusions can be drawn from these biophysical simulations. First, the effect of surfactant concentration on the dynamic surface activity of the Infasurf film appears to be only important for the physiologically relevant compression ratio of 15%. For 25% and 35% compression ratios, no statistically significant differences between the γ_{min} and κ_{comp} can be found for surfactant concentrations between 1 and 35 mg/mL. Numerous lung physiological studies have demonstrated that variations in the alveolar surface area during normal tidal breathing are less than 20% and usually no more than 30% for a deep breath (13, 32, 33). In contrast to the 15% compression ratio (Fig. 2*A*), the compression-expansion cycles with 25% and 35% compression ratios (Fig. 2, *D* and *G*) show apparent hysteresis areas. The hysteresis between the compression and expansion branches is a result of reversible film collapse (34), when the surfactant film is compressed beyond 20% of its initial surface area, at which the surface tension remains constant in spite of film compression. Such a phenomenon in in vitro biophysical simulations of pulmonary surfactant is termed "overcompression" of the surfactant film (17, 35), which is unlikely to occur in vivo during normal tidal breathing since the hysteresis area indicates energy loss per cycle due to partial collapse of the surfactant film (1). The hysteresis area, i.e., the energy loss, for the Infasurf film at 15%, 25%, and 35% compression ratios are calculated to be ~0.01, 0.05, and 0.09 μJ/cycle, respectively.

Second, at the physiologically relevant 15% compression ratio, the compressibility (κ_{comp}) of the Infasurf film decreases with increasing surfactant concentration from 1 to 35 mg/mL. Film compressibility measures the "hardness" of a two-dimensional film, with a lower compressibility indicating a "harder" film since the film is less compressible (36). Hence, these data suggest that the adsorbed Infasurf film becomes harder with increasing surfactant concentration. This is an interesting finding because it indicates that the surfactant concentration in the subphase influences the

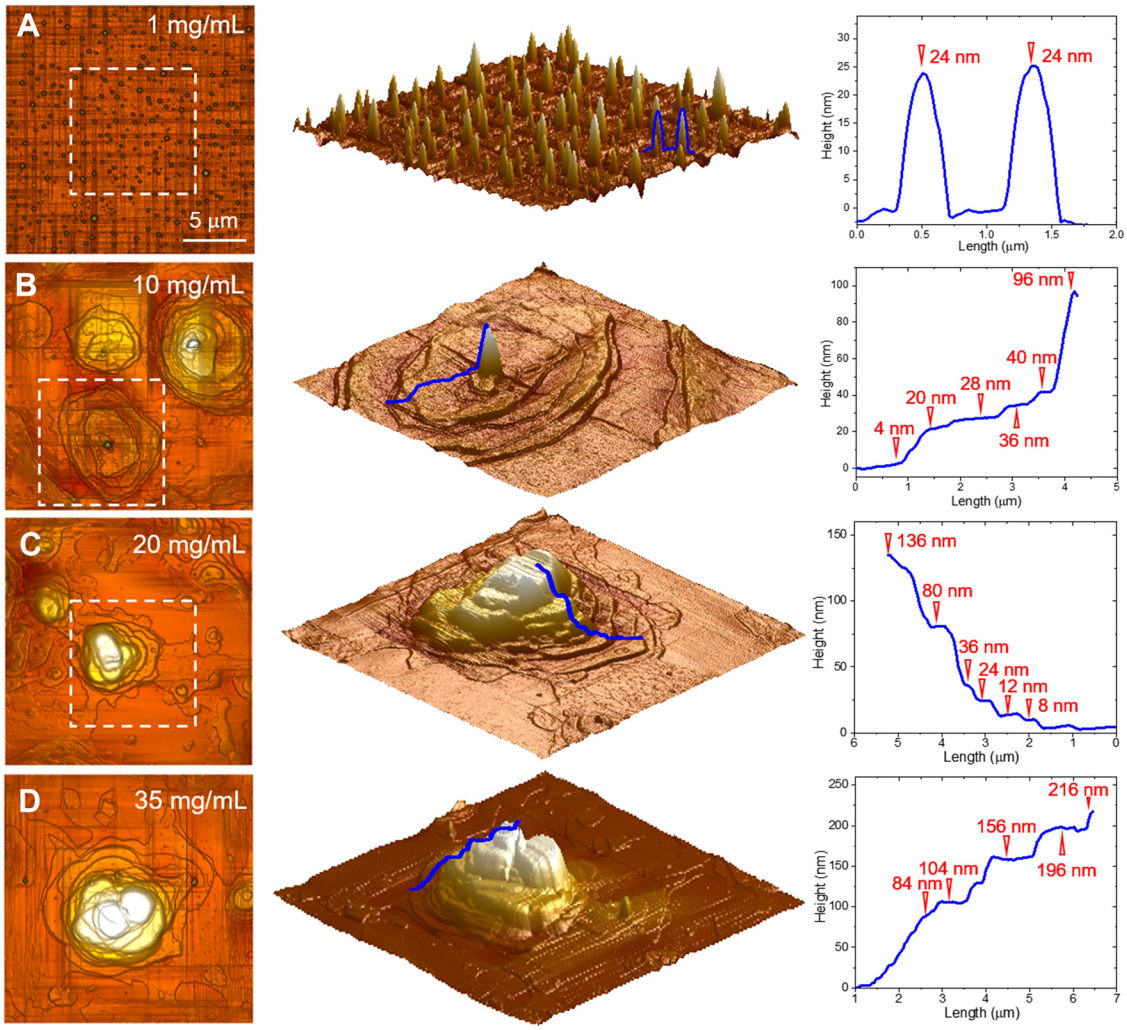

Figure 4. Ultrastructure and topography of the Infasurf film after de novo adsorption from phospholipid concentrations of 1 mg/mL (*A*), 10 mg/mL (*B*), 20 mg/mL (*C*), and 35 mg/mL (*D*). All atomic force microscopy (AFM) images were obtained with optimal subphase replacement conditions demonstrated in Fig. 3 and Supplemental Fig. S12. Images in the *left* column show the topographic map of the Infasurf film adsorbed from various surfactant concentrations. Each contour line of the topographic map connects points of equal height of the multilayers. All images have the same scanning area of 20 × 20 μm. The *z* range is 150 nm for images in *A* and *B*, and 400 nm for images in *C* and *D*. Images in the *middle* column show the three-dimensional (3-D) rendering of the adsorbed Infasurf films, indicated inside the white boxes shown in the images on the *left*. To better illustrate the multilayer structures, the corresponding topographic map was rotated in the clockwise direction by 45°. Images in the *right* column show the height profile of the multilayer structures indicated by the blue lines superimposed onto the 3-D rendering of the adsorbed Infasurf film.

dynamic surface activity of the surfactant film after de novo adsorption at the air-water surface. Similar findings have been reported in the literature (35, 37–39), but the biophysical mechanism responsible for the synergetic effect of the surfactant concentration on the surface activity of the surfactant film is still unknown (40). Recently, using grazing incidence X-ray diffraction (GIXD), Andreev et al. (41) showed that increasing the subphase concentration of an Infasurf film in a Langmuir film balance increases the lateral area of an ordered phase in the surfactant film at the air-water surface. This ordered phase resembles the properties of a DPPC:cholesterol (3:1) monolayer (41), thus indicating that it is the liquid-ordered (LO) phase in the surfactant monolayer (1). Consequently, the decreased film compressibility at high surfactant concentration found here might be, at least in part, due to the formation of more LO phase at the interfacial monolayer. It should also be noted that although the compressibility appears to increase with increasing the film compression ratio from 15% to 35% (Fig. 2*C* vs. *F* and *I*), it most likely does not indicate that the surfactant film becomes "softer" with increasing compression ratio. This is because the evaluation of film compressibility assumes no molecules leave the surface, i.e., no film collapse (36). Hence, the increase in film compressibility when increasing the compression ratio to 25% and 35% is most likely linked to film collapse instead of the hardness of the surfactant film.

Multilayers of the Adsorbed Surfactant Film Act as a Safety Net for Deep Breathing

Many in vitro studies have directly and indirectly demonstrated that the adsorbed pulmonary surfactant film has a complex conformation, consisting of an interfacial monolayer at the air-water surface and phospholipid multilayers

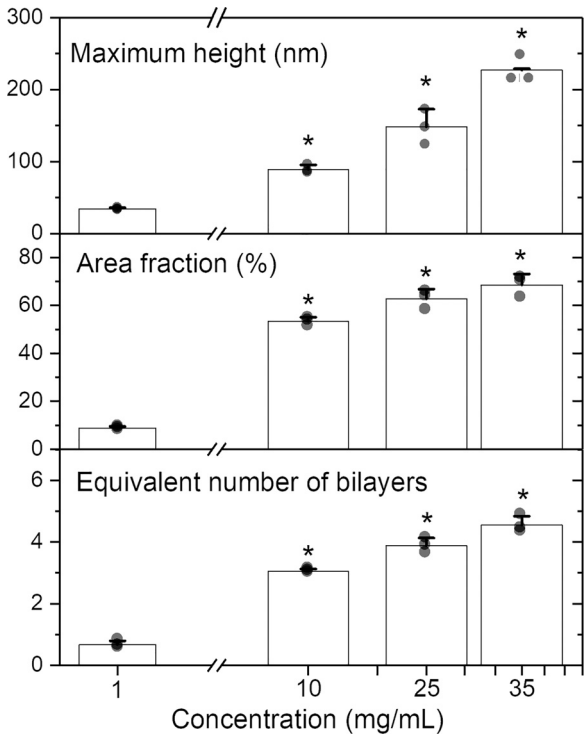

Figure 5. Maximum height (nm), area fraction (%), and the area-averaged equivalent number of bilayers of the multilayer structures of the Infasurf film adsorbed from various subphase concentrations from 1 to 35 mg/mL. The equivalent number of bilayers stored in the multilayers was determined from bearing analysis of the atomic force microscopy (AFM) topographic images (see Supplemental Fig. S12 for technical details). *P <0.05 in comparison with Infasurf at the phospholipid concentration of 1 mg/mL.

closely and functionally fused with the interfacial monolayer (3, 27, 42–46). Hydrophobic surfactant proteins (SP-B and SP-C) likely play an important role in stabilizing the negative curvatures needed for membrane fusion (39, 47–49). Such a monolayer-multilayer fusion structure facilitates the rapid exchange of surface-active materials between the monolayer and the multilayer, upon highly dynamic compression-expansion cycles of the surfactant film during normal tidal breathing (50, 51). Under pathophysiological conditions of protein denaturation, such as exposure to excessive nanoparticles (52, 53) or menthol-flavored e-cigarette aerosols (54, 55), it was found that the multilayer structure of the natural pulmonary surfactant film was compromised and downgraded into a monolayer confirmation. The change of surfactant film conformation was found to be associated with in vitro biophysical inhibition of the surfactant film and acute respiratory failure in animal models (56–58).

The present study showed that the ultrastructure and topography of the adsorbed Infasurf film depend on the phospholipid concentration of the surfactant suspension (Figs. 4 and 5). The multilayers of the Infasurf film adsorbed from a surfactant concentration of only 1 mg/mL appear as individual spear-like protrusions uniformly distributed throughout the surface of the surfactant film (Fig. 4*A*). Although each of these protrusions could account for up to nine stacked phospholipid bilayers, since they only have a limited surface coverage (< 10%), the area-averaged equivalent number of phospholipid bilayers stored in these multilayers was found to be only 0.7 (Fig. 5).

Using transmission electron microscopy (TEM), Schürch et al. (16) and Ochs (59) have shown convincing evidence that a large portion of the surfactant film adsorbed to the air-water surface of the alveolar-lining layer appears to be multilayers with a varying number of 2–7 bilayers. AFM images shown in the present study depict that the Infasurf film adsorbed from physiologically relevant high surfactant concentrations (between 10 and 35 mg/mL) are multilayers with an area-averaged number of 3–5 bilayers (Fig. 5). These AFM observations are in good agreement with the TEM observations of the surfactant film at the alveolar lining layer (16, 59).

Interestingly, it appears that the biophysical function of the excessive lipids stored in the multilayers at high surfactant concentrations is not to increase the dynamic surface activity of the adsorbed surfactant film when the surface area compression ratio is increased to supraphysiological levels (i.e., 25% and 35% shown in Fig. 2). Rather, the beneficial effect of the high surfactant concentration on surface activity of the adsorbed Infasurf film only appears to be significant at the physiologically relevant 15% compression ratio, at which no collapse of the interfacial monolayer occurs at the end of compression (Fig. 2, *A*–*C*). These experimental results likely indicate that the biophysical function of these multilayer structures formed after de novo adsorption is to act as a buffer zone to store surface-active materials ejected from the interfacial monolayer under extreme conditions such as deep breathing or forced breathing. Under these conditions, the surfactant film is stretched beyond its normal compression ratio, which occurs at the expense of partial collapse of the interfacial surfactant film (Fig. 2, *D* and *G*). Instead of losing these surface-active materials to the subphase, e.g., in the form of small vesicular aggregates (60), these materials can be temporarily absorbed by and stored in the adsorbed multilayer structures. As a result, these materials can respread back to the interfacial monolayer sufficiently fast so that low surface tensions can be achieved in the subsequent respiratory cycle immediately following a deep breath.

In conclusion, using constrained drop surfactometry (CDS), we have studied the biophysical properties, ultrastructure, and topography of the pulmonary surfactant film adsorbed from the subphase at physiologically relevant high surfactant concentrations (i.e., 10–35 mg/mL). It was found that the effect of surfactant concentration on the dynamic surface activity of the Infasurf film was only important for the physiologically relevant compression ratio of 15%. For supraphysiological compression ratios, at which the surfactant film partially collapses at the end of compression, no statistically significant differences in the minimum surface tension and film compressibility can be found between these high surfactant concentrations and a relatively low concentration of 1 mg/mL. Atomic force microscopy (AFM) observed that the adsorbed Infasurf film depicts a multilayer conformation consisting of layer-by-layer assembly of stacked bilayers with the height of the multilayers proportional to the surfactant concentration in the subphase. At 35 mg/mL, the phospholipids stored in these multilayer structures are equivalent to 4.6 lipid bilayers throughout the entire surfactant film. Our experimental data

suggest that the biophysical function of these multilayer structures formed after de novo adsorption is to act as a buffer zone to store surface-active materials ejected from the interfacial monolayer under extreme conditions such as deep breathing.

DATA AVAILABILITY

Data will be made available upon reasonable request.

SUPPLEMENTAL DATA

Supplemental Figs. S1–S12: https://doi.org/10.6084/m9.figshare.22359907.

ACKNOWLEDGMENTS

We thank Dr. Sindhu Row of ONY Biotech for donation of Infasurf samples.

GRANTS

This research was supported by the National Science Foundation Grant No. CBET-2011317 (Y.Y.Z.).

DISCLOSURES

No conflicts of interest, financial or otherwise, are declared by the authors.

AUTHOR CONTRIBUTIONS

Y.Y.Z. conceived and designed research; X.X. and G.L. performed experiments; X.X. analyzed data; X.X. and Y.Y.Z. interpreted results of experiments; X.X. prepared figures; X.X. and Y.Y.Z. drafted manuscript; Y.Y.Z. edited and revised manuscript; Y.Y.Z. approved final version of manuscript.

REFERENCES

1. **Zuo YY**, **Veldhuizen RA**, **Neumann AW**, **Petersen NO**, **Possmayer F.** Current perspectives in pulmonary surfactant–inhibition, enhancement and evaluation. *Biochim Biophys Acta* 1778: 1947–1977, 2008. doi:10.1016/j.bbamem.2008.03.021.
2. **Thébaud B**, **Goss KN**, **Laughon M**, **Whitsett JA**, **Abman SH**, **Steinhorn RH**, **Aschner JL**, **Davis PG**, **McGrath-Morrow SA**, **Soll RF**, **Jobe AH.** Bronchopulmonary dysplasia. *Nat Rev Dis Primers* 5: 78, 2019. doi:10.1038/s41572-019-0127-7.
3. **Castillo-Sánchez JC**, **Cruz A**, **Pérez-Gil J.** Structural hallmarks of lung surfactant: lipid-protein interactions, membrane structure and future challenges. *Arch Biochem Biophys* 703: 108850, 2021. doi:10.1016/j.abb.2021.108850.
4. **Whitsett JA**, **Stahlman MT.** Impact of advances in physiology, biochemistry, and molecular biology on pulmonary disease in neonates. *Am J Respir Crit Care Med* 157: S67–S71, 1998. doi:10.1164/ajrccm.157.4.nhlb1-2.
5. **Clements JA**, **Avery ME.** Lung surfactant and neonatal respiratory distress syndrome. *Am J Respir Crit Care Med* 157: S59–S66, 1998. doi:10.1164/ajrccm.157.4.nhlb1-1.
6. **Polin RA**, **Carlo WA**; **Committee on Fetus and Newborn; Papile L-A**, **Polin RA**, **Carlo W**, **Tan R**, **Kumar P**, **Benitz W**, **Eichenwald E**, **Cummings J**, **Baley J.** Surfactant replacement therapy for preterm and term neonates with respiratory distress. *Pediatrics* 133: 156–163, 2014. doi:10.1542/peds.2013-3443.
7. **Lewis JF**, **Veldhuizen R.** The role of exogenous surfactant in the treatment of acute lung injury. *Annu Rev Physiol* 65: 613–642, 2003. doi:10.1146/annurev.physiol.65.092101.142434.
8. **Kneyber MCJ**, **Khemani RG**, **Bhalla A**, **Blokpoel RGT**, **Cruces P**, **Dahmer MK**, **Emeriaud G**, **Grunwell J**, **Ilia S**, **Katira BH**, **Lopez-Fernandez YM**, **Rajapreyar P**, **Sanchez-Pinto LN**, **Rimensberger PC.** Understanding clinical and biological heterogeneity to advance precision medicine in paediatric acute respiratory distress syndrome. *Lancet Respir Med* 11: 197–212, 2023. doi:10.1016/S2213-2600(22)00483-0.
9. **Veldhuizen RAW**, **Zuo YY**, **Petersen NO**, **Lewis JF**, **Possmayer F.** The COVID-19 pandemic: a target for surfactant therapy? *Expert Rev Respir Med* 15: 597–608, 2021. doi:10.1080/17476348.2021.1865809.
10. **Zuo YY**, **Uspal WE**, **Wei T.** Airborne transmission of COVID-19: aerosol dispersion, lung deposition, and virus-receptor interactions. *ACS Nano* 14: 16502–16524, 2020. doi:10.1021/acsnano.0c08484.
11. **Enhorning G.** Pulsating bubble technique for evaluating pulmonary surfactant. *J Appl Physiol Respir Environ Exerc Physiol* 43: 198–203, 1977. doi:10.1152/jappl.1977.43.2.198.
12. **Enhorning G.** Pulmonary surfactant function studied with the pulsating bubble surfactometer (PBS) and the capillary surfactometer (CS). *Comp Biochem Physiol A Mol Integr Physiol* 129: 221–226, 2001. doi:10.1016/s1095-6433(01)00318-x.
13. **Bachofen H**, **Schürch S**, **Urbinelli M**, **Weibel ER.** Relations among alveolar surface tension, surface area, volume, and recoil pressure. *J Appl Physiol (1985)* 62: 1878–1887, 1987. doi:10.1152/jappl.1987.62.5.1878.
14. **Schürch S**, **Bachofen H**, **Goerke J**, **Possmayer F.** A captive bubble method reproduces the in situ behavior of lung surfactant monolayers. *J Appl Physiol (1985)* 67: 2389–2396, 1989. doi:10.1152/jappl.1989.67.6.2389.
15. **Schürch S**, **Bachofen H**, **Goerke J**, **Green F.** Surface properties of rat pulmonary surfactant studied with the captive bubble method: adsorption, hysteresis, stability. *Biochim Biophys Acta* 1103: 127–136, 1992. doi:10.1016/0005-2736(92)90066-u.
16. **Schürch S**, **Green FH**, **Bachofen H.** Formation and structure of surface films: captive bubble surfactometry. *Biochim Biophys Acta* 1408: 180–202, 1998. doi:10.1016/s0925-4439(98)00067-2.
17. **Schürch S**, **Bachofen H**, **Possmayer F.** Surface activity in situ, in vivo, and in the captive bubble surfactometer. *Comp Biochem Physiol A Mol Integr Physiol* 129: 195–207, 2001. doi:10.1016/s1095-6433(01)00316-6.
18. **Zuo YY**, **Ding M**, **Li D**, **Neumann AW.** Further development of axisymmetric drop shape analysis-captive bubble for pulmonary surfactant related studies. *Biochim Biophys Acta* 1675: 12–20, 2004. doi:10.1016/j.bbagen.2004.08.003.
19. **Zuo YY**, **Do C**, **Neumann AW.** Automatic measurement of surface tension from noisy images using a component labeling method. *Colloids Surf A Physicochem Eng Asp* 299: 109–116, 2007. doi:10.1016/j.colsurfa.2006.11.027.
20. **Codd JR**, **Schürch S**, **Daniels CB**, **Orgeig S.** Torpor-associated fluctuations in surfactant activity in Gould's wattled bat. *Biochim Biophys Acta* 1580: 57–66, 2002. doi:10.1016/s1388-1981(01)00185-8.
21. **Lewis JF**, **Jobe AH.** Surfactant and the adult respiratory distress syndrome. *Am Rev Respir Dis* 147: 218–233, 1993 [Erratum in *Am Rev Respir Dis* 147: 1068, 1993]. doi:10.1164/ajrccm/147.1.218.
22. **Ikegami M**, **Rebello CM**, **Jobe AH.** Surfactant inhibition by plasma: gestational age and surfactant treatment effects in preterm lambs. *J Appl Physiol (1985)* 81: 2517–2522, 1996. doi:10.1152/jappl.1996.81.6.2517.
23. **Rebello CM**, **Jobe AH**, **Eisele JW**, **Ikegami M.** Alveolar and tissue surfactant pool sizes in humans. *Am J Respir Crit Care Med* 154: 625–628, 1996. doi:10.1164/ajrccm.154.3.8810596.
24. **Weibel ER.** Morphological basis of alveolar-capillary gas exchange. *Physiol Rev* 53: 419–495, 1973. doi:10.1152/physrev.1973.53.2.419.
25. **Bastacky J**, **Lee CY**, **Goerke J**, **Koushafar H**, **Yager D**, **Kenaga L**, **Speed TP**, **Chen Y**, **Clements JA.** Alveolar lining layer is thin and continuous: low-temperature scanning electron microscopy of rat lung. *J Appl Physiol (1985)* 79: 1615–1628, 1995. doi:10.1152/jappl.1995.79.5.1615.
26. **Valle RP**, **Wu T**, **Zuo YY.** Biophysical influence of airborne carbon nanomaterials on natural pulmonary surfactant. *ACS Nano* 9: 5413–5421, 2015. doi:10.1021/acsnano.5b01181.
27. **Xu L**, **Yang Y**, **Zuo YY.** Atomic force microscopy imaging of adsorbed pulmonary surfactant films. *Biophys J* 119: 756–766, 2020. doi:10.1016/j.bpj.2020.06.033.
28. **Zuo YY**, **Chen R**, **Wang X**, **Yang J**, **Policova Z**, **Neumann AW.** Phase transitions in dipalmitoylphosphatidylcholine monolayers. *Langmuir* 32: 8501–8506, 2016. doi:10.1021/acs.langmuir.6b01482.

29. **Yu K**, **Yang J**, **Zuo YY.** Automated droplet manipulation using closed-loop axisymmetric drop shape analysis. *Langmuir* 32: 4820–4826, 2016. doi:10.1021/acs.langmuir.6b01215.
30. **Cruz A**, **Pérez-Gil J.** Langmuir films to determine lateral surface pressure on lipid segregation. *Methods Mol Biol* 400: 439–457, 2007. doi:10.1007/978-1-59745-519-0_29.
31. **Marsh D.** *CRC Handbook of Lipid Bilayers*. Boca Raton, FL: CRC Press, 1990.
32. **Bachofen H**, **Schürch S.** Alveolar surface forces and lung architecture. *Comp Biochem Physiol A Mol Integr Physiol* 129: 183–193, 2001. doi:10.1016/s1095-6433(01)00315-4.
33. **Kharge AB**, **Wu Y**, **Perlman CE.** Surface tension in situ in flooded alveolus unaltered by albumin. *J Appl Physiol (1985)* 117: 440–451, 2014. doi:10.1152/japplphysiol.00084.2014.
34. **Schürch S**, **Schürch D**, **Curstedt T**, **Robertson B.** Surface activity of lipid extract surfactant in relation to film area compression and collapse. *J Appl Physiol (1985)* 77: 974–986, 1994. doi:10.1152/jappl.1994.77.2.974.
35. **Dagan MP**, **Hall SB.** The equilibrium spreading tension of pulmonary surfactant. *Langmuir* 31: 13063–13067, 2015. doi:10.1021/acs.langmuir.5b03094.
36. **Gaines GL.** *Insoluble Monolayers at Liquid-Gas Interfaces*. New York: Interscience Publishers, 1966.
37. **Putz G**, **Goerke J**, **Clements JA.** Surface activity of rabbit pulmonary surfactant subfractions at different concentrations in a captive bubble. *J Appl Physiol (1985)* 77: 597–605, 1994. doi:10.1152/jappl.1994.77.2.597.
38. **Veldhuizen EJ**, **Batenburg JJ**, **van Golde LM**, **Haagsman HP.** The role of surfactant proteins in DPPC enrichment of surface films. *Biophys J* 79: 3164–3171, 2000. doi:10.1016/S0006-3495(00)76550-7.
39. **Schürch D**, **Ospina OL**, **Cruz A**, **Pérez-Gil J.** Combined and independent action of proteins SP-B and SP-C in the surface behavior and mechanical stability of pulmonary surfactant films. *Biophys J* 99: 3290–3299, 2010. doi:10.1016/j.bpj.2010.09.039.
40. **Rugonyi S**, **Biswas SC**, **Hall SB.** The biophysical function of pulmonary surfactant. *Respir Physiol Neurobiol* 163: 244–255, 2008. doi:10.1016/j.resp.2008.05.018.
41. **Andreev K**, **Martynowycz MW**, **Kuzmenko I**, **Bu W**, **Hall SB**, **Gidalevitz D.** Structural changes in films of pulmonary surfactant induced by surfactant vesicles. *Langmuir* 36: 13439–13447, 2020. doi:10.1021/acs.langmuir.0c01813.
42. **Diemel RV**, **Snel MM**, **Waring AJ**, **Walther FJ**, **van Golde LM**, **Putz G**, **Haagsman HP**, **Batenburg JJ.** Multilayer formation upon compression of surfactant monolayers depends on protein concentration as well as lipid composition an atomic force microscopy study. *J Biol Chem* 277: 21179–21188, 2002. doi:10.1074/jbc.M111758200.
43. **Yu SH**, **Possmayer F.** Lipid compositional analysis of pulmonary surfactant monolayers and monolayer-associated reservoirs. *J Lipid Res* 44: 621–629, 2003. doi:10.1194/jlr.M200380-JLR200.
44. **Alonso C**, **Alig T**, **Yoon J**, **Bringezu F**, **Warriner H**, **Zasadzinski JA.** More than a monolayer: relating lung surfactant structure and mechanics to composition. *Biophys J* 87: 4188–4202, 2004. doi:10.1529/biophysj.104.051201.
45. **Bachofen H**, **Gerber U**, **Gehr P**, **Amrein M**, **Schürch S.** Structures of pulmonary surfactant films adsorbed to an air-liquid interface in vitro. *Biochim Biophys Acta* 1720: 59–72, 2005. doi:10.1016/j.bbamem.2005.11.007.
46. **Schürch S**, **Qanbar R**, **Bachofen H**, **Possmayer F.** The surface -associated surfactant reservoir in the alveolar lining. *Biol Neonate* 67, *Suppl* 1: 61–76, 1995. doi:10.1159/000244207.
47. **Martínez-Calle M**, **Parra-Ortiz E**, **Cruz A**, **Olmeda B**, **Pérez-Gil J.** Towards the molecular mechanism of pulmonary surfactant protein SP-B: at the crossroad of membrane permeability and interfacial lipid transfer. *J Mol Biol* 433: 166749, 2021. doi:10.1016/j.jmb.2020.166749.
48. **Sachan AK**, **Zasadzinski JA.** Interfacial curvature effects on the monolayer morphology and dynamics of a clinical lung surfactant. *Proc Natl Acad Sci USA* 115: E134–E143, 2018. doi:10.1073/pnas.1715830115.
49. **Chavarha M**, **Loney RW**, **Rananavare SB**, **Hall SB.** Hydrophobic surfactant proteins strongly induce negative curvature. *Biophys J* 109: 95–105, 2015. doi:10.1016/j.bpj.2015.05.030.
50. **Amrein M**, **von Nahmen A**, **Sieber M.** A scanning force- and fluorescence light microscopy study of the structure and function of a model pulmonary surfactant. *Eur Biophys J* 26: 349–357, 1997. doi:10.1007/s002490050089.
51. **Galla HJ**, **Bourdos N**, **Von Nahmen A**, **Amrein M**, **Sieber M.** The role of pulmonary surfactant protein C during the breathing cycle. *Thin Solid Films* 327–329: 632–635, 1998. doi:10.1016/S0040-6090(98)00728-7.
52. **Fan Q**, **Wang YE**, **Zhao X**, **Loo JS**, **Zuo YY.** Adverse biophysical effects of hydroxyapatite nanoparticles on natural pulmonary surfactant. *ACS Nano* 5: 6410–6416, 2011. doi:10.1021/nn2015997.
53. **Yang Y**, **Xu L**, **Dekkers S**, **Zhang LG**, **Cassee FR**, **Zuo YY.** Aggregation state of metal-based nanomaterials at the pulmonary surfactant film determines biophysical inhibition. *Environ Sci Technol* 52: 8920–8929, 2018. doi:10.1021/acs.est.8b02976.
54. **Xu L**, **Yang Y**, **Simien JM**, **Kang C**, **Li G**, **Xu X**, **Haglund E**, **Sun R**, **Zuo YY.** Menthol in electronic cigarettes causes biophysical inhibition of pulmonary surfactant. *Am J Physiol Lung Cell Mol Physiol* 323: L165–L177, 2022. doi:10.1152/ajplung.00015.2022.
55. **Graham E**, **McCaig L**, **Shui-Kei Lau G**, **Tejura A**, **Cao A**, **Zuo YY**, **Veldhuizen R.** E-cigarette aerosol exposure of pulmonary surfactant impairs its surface tension reducing function. *PLoS One* 17: e0272475, 2022. doi:10.1371/journal.pone.0272475.
56. **Yang Y**, **Wu Y**, **Ren Q**, **Zhang LG**, **Liu S**, **Zuo YY.** Biophysical assessment of pulmonary surfactant predicts the lung toxicity of nanomaterials. *Small Methods* 2: 1700367, 2018. doi:10.1002/smtd.201700367.
57. **Chen Y**, **Yang Y**, **Xu B**, **Wang S**, **Li B**, **Ma J**, **Gao J**, **Zuo YY**, **Liu S.** Mesoporous carbon nanomaterials induced pulmonary surfactant inhibition, cytotoxicity, inflammation and lung fibrosis. *J Environ Sci (China)* 62: 100–114, 2017. doi:10.1016/j.jes.2017.08.018.
58. **Da Silva E**, **Vogel U**, **Hougaard KS**, **Pérez-Gil J**, **Zuo YY**, **Sørli JB.** An adverse outcome pathway for lung surfactant function inhibition leading to decreased lung function. *Curr Res Toxicol* 2: 225–236, 2021. doi:10.1016/j.crtox.2021.05.005.
59. **Ochs M.** The closer we look the more we see? Quantitative microscopic analysis of the pulmonary surfactant system. *Cell Physiol Biochem* 25: 27–40, 2010. doi:10.1159/000272061.
60. **Goerke J.** Pulmonary surfactant: functions and molecular composition. *Biochim Biophys Acta* 1408: 79–89, 1998. doi:10.1016/s0925-4439(98)00060-x.